Deep Learning for Ionogram Parameter Extraction: A Time-Series Approach to Ionospheric Monitoring

A. Castro[1*], P. Condor[1†], D. Scipion[1‡] and E. Pacheco[1§]

[1]Instituto Geofísico del Perú, Lima, Perú.

Corresponding author: Armando Castro (acastro@igp.gob.pe)

Key Points:

- Machine learning model to estimate frequency profiles from VIPIR ionograms.
- Automated ionospheric monitoring enhanced by ionogram-based machine learning.
- The performance of the automatic scaled ionograms was improved by treating the estimation as a time series of ionograms and incorporating an LSTM layer into our model.

Abstract

Ionograms provide a direct measurement of the ionosphere's electron density profile and its irregularities. By examining critical frequencies researchers can identify key parameters—such as the F-region critical frequency (foF2), the height of maximum electron density (hmF2), and the presence of Spread-F irregularities—that are vital for understanding signal propagation, space-weather effects, and radio-communication reliability. Over the past decades, tools have been developed for the extraction of ionospheric parameters of ionograms: ARTIST-5 and among others. There are approximations in previous works using deep learning for automatic scaling with parameters extraction of great importance as the identification of the E and F2 layer. These tools generally work for relatively quiet days (QD), but not for days with Spread-F, where a lot of variability is observed in the parameters obtained in those days and manual correction is necessary. In this work, we trained a model combining Convolutional Neuronal Network (CNN), Long Short-Term Memory (LSTM) and Dense layers that can capture the short-term variability of the ionosphere and our model returns the frequency profile. Ionograms were recollected from VIPIR ionosondes, part of the Low-Latitude Ionospheric Sensor Network (LISN). We tested and compared the frequency profiles from our model with manual correction and parameters obtained with ARTIST 5.0 showing significant differences.

[*] acastro@igp.gob.pe
[†] pcondor@igp.gob.pe
[‡] dscipion@igp.gob.pe
[§] epacheco@igp.gob.pe

1. Introduction

The Jicamarca Radio Observatory (JRO), a facility of the Geophysical Institute of Peru (IGP), began operations in 1961 with the largest incoherent scatter and powerful radar in the world. Over the years, the observatory has acquired additional instruments to improve the study and monitoring of the ionosphere. In 1983, the first digisonde was acquired, providing valuable data for interpretation and studies. In 2022, the ionosonde failed and was replaced by a VIPIR ionosonde from the Low Latitude Ionospheric Sensor Network (LISN).

LISN is a distributed observatory equipped with various instruments, including GNSS receivers, VIPIR ionosondes, magnetometers, and others, with the primary goal of obtaining parameters of the low-latitude ionosphere (Gopi Krishna et al., 2009; Valladares & Chau, 2012) . VIPIR ionosondes generate 244 ionograms per day every five minutes at each station.

Spread-F is an ionospheric anomaly that frequently occurs in the equatorial region but can also be observed at low latitudes, causing significant contamination in ionograms. According to (Penndorf, 1962; G. Wang et al., 2008), ionograms can be classified into clear, Frequency Spread-F (FSF), Range Spread-F (RSF), Strong Spread-F (SSF), and undefined categories.

Manually scaling ionograms daily is a highly demanding task, especially given the difficulty in distinguishing the correct reflection layer in ionogram values when ionograms contain Spread-F. ARTIST 5.0 developed and explained in (Galkin et al., 2008), is an important tool for automatic ionogram scaling and comes built into the SAOExplorer software. This method reduces the workload for operators; however, it faces significant challenges with the presence of Spread-F anomalies. At IGP, ionograms are scaled automatically with ARTIST 5.0 and recorded jointly with SAO file.

When data is necessary for a type of study or requested by a researcher, each ionogram is corrected manually with SAOExplorer. The operator analyzes previous ionograms to detect oscillations in the foF2 value. This approach allows us to estimate and approximate where is the foF2 for the current ionogram. By leveraging this method, we would suggest that scaling estimation follows a sequential or time-series pattern.

In Machine Learning area, Convolutional Neuronal Networks (CNNs) have demonstrated strong generalization capabilities in pattern recognition tasks across various applications. They have been effectively combined with Long Short-Term Memory (LSTM) (Graves & Graves, 2012; Kim et al., 2017) and forward dense layers for tasks such as video classification (Abdullah et al., 2020), video tagging (X. Wang et al., 2016), weather forecasting (Gong et al., 2024), remote sensing (Pan et al., 2023) and other applications involving spatial and temporal data (Alshingiti et al., 2023).

Several studies have successfully used CNNs to classify ionograms affected by Spread-F with high accuracy in an automatic manner (Benchawattananon et al., 2024; Yacoub et al., 2025). Another application using CNN layers has been ionogram filtering to isolate reflections from the E and F layers of the ionospher (De la Jara & Olivares, 2021). Extraction of parameters of ionograms using deep learning has been developed in (Sherstyukov et al., 2024; Xiao et al., 2020), presenting important results. However, these approaches typically treat ionograms as independent 2D images and do not incorporate sequential processing.

In contrast, our work introduces a sequential analysis that leverages the natural frequency ordering of ionograms in our Machine Learning (ML) model. This allows the model to better capture the physical consistency of the extracted parameters and to reduce the need for manual corrections, regardless of the presence of Spread-F. Our model is capable of generating frequency profiles from ionograms using five consecutive ionograms, improving robustness and continuity in parameter estimation.

This paper is organized as follows: Sections 2.1 and 2.2 describe the data collection and preprocessing procedures. Section 2.3 introduces the proposed model and the training process using our dataset. Section 3 presents the results and comparisons for time intervals affected by Spread-F events and storm magnetic. In this section, we compare the hmF2 and foF2 parameters estimated by our model and compute the corresponding errors. Finally, Section 4 summarizes the conclusions and provides recommendations based on the findings of this study.

2. Method

2.1. Data recollection

The data used in this study were collected from VIPIR ionosondes. At the time of writing, only two VIPIR ionosondes are operational: one located in Tucumán, Argentina (26.84°S, 65.23°W), and another in Jicamarca, Peru (11.952°S, 76.876°W). For this work, we used only data collected from the Jicamarca ionosonde.

The dataset spans multiple years and has been scaled and manually corrected using the SAOExplorer software. The corrected data were saved in SAO file format. Each day includes at least one ionogram affected by some type of Spread-F anomaly.

Table 1 provides a summary of the available years, including the number of ionograms per year and the total count. Typically, 244 ionograms were recorded per day. However, in 2024, the ionosonde configuration was modified for a specific experiment, resulting in 1,440 ionograms per day. In total, the dataset includes 15,520 ionograms.

Table 1. Description of data for year.

Year	**Day of year**	**# Ionograms**
2017	233 y 234	488
2019	81,82,83,84,85,86 y 87	1708
2020	14, 15, 16,17, 18, 19, 20, 21, 22, 56, 57, 58, 59 y 60	3416
2022	15 y 16	488
2023	23,25,26,27,34,54,55,56,57,58,59,60,61,62 y 276	3660
2024	149, 150, 151 y 152	5760
Total		15520

2.2. Data preprocessing and preparing dataset

An ionogram contains data from both ordinary (O) and extraordinary (X) polarizations. Each ionogram was transformed into a $256 \times 256 \times 2$ array, where the first and second dimensions represent frequency (ranging from 0 to 22 MHz) and virtual height (ranging from 0 to 1000 kilometers), and the third dimension corresponds to the polarization.

For noise removal, we applied a threshold filter that discards points with a signal strength below 20 dB. Values exceeding 50 dB were clipped to 50 dB, then values was linearized to range in 0 to 255. Representative image of transformation is showed in Figure 1.

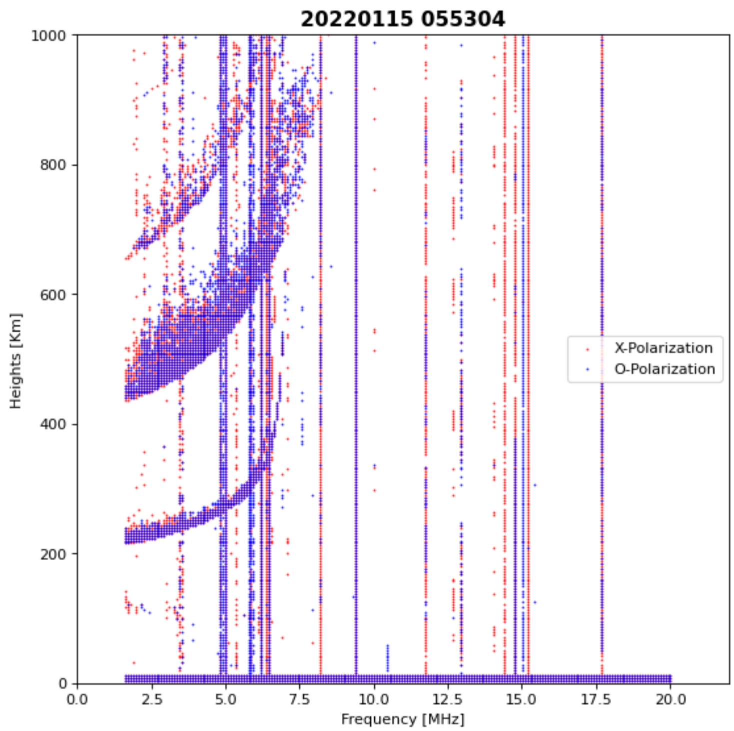

Figure 1. X and O mode polarizations shown in a 256 × 256 pixel image, with frequency ranging from 0 to 22 MHz and height from 0 to 1000 km.

For each ionogram, we incorporate multiple preceding ionograms to help mitigate inconsistencies caused by anomalies. In this work, we use five consecutive ionograms as input to train the machine learning model, with the target frequency profile corresponding to the last ionogram in the sequence. The target frequency profiles were extracted from SAO files (corresponding to the current ionogram) and transformed into 256-element arrays ranging 0 to 1000 km. These values range from 0 to 25 MHz.

Our dataset has dimensions of 4 × 5 × 256 × 256 × 2 when using a batch size of 4, and the corresponding target data has dimensions of 4 × 256. The dataset was saved in HDF5 (h5) format.

2.3. Model description and training

Our regression ML model combines CNN, LSTM and Dense layers (Figure 2 Description of the machine learning model combining ResNet units, an LSTM layer, and a Dense layer output). Using CNN layers in our model will serve as a filter to extract useful representations and patterns in an automatic manner from ionograms (De la Jara & Olivares, 2021). Since ionogram scaling can be approached as a time series problem-due need to check previous ionogram-we incorporate an LSTM layer. The architecture of our model is described in , where we explain each layer and output in detail.

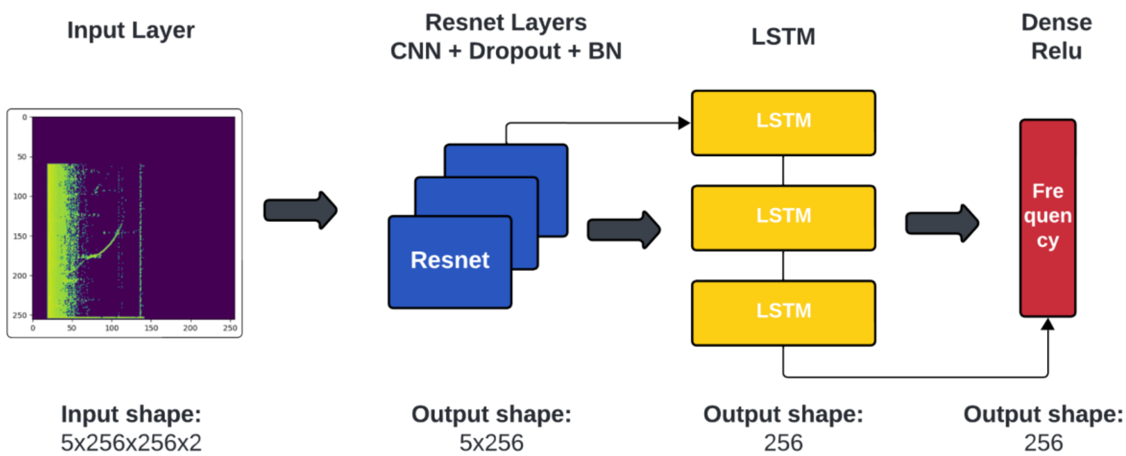

Figure 2. Description of the machine learning model combining ResNet units, an LSTM layer, and a Dense layer output. Input has 5x256x256x2 size and frequency values as output has 256 values.

The proposed model has over 5.5 million parameters, which is relatively high compared to the number of collected ionograms. To increase data diversity in each training epoch and prevent the model from overfitting, we apply regularization techniques such as Batch Normalization, Dropout, and Weight Regularization (Santos & Papa, 2022; Srivastava et al., 2014). Additionally for regularization, Gaussian noise with a standard deviation of 0.01 and mean of 0 is added in input to each batch (Moradi et al., 2020).

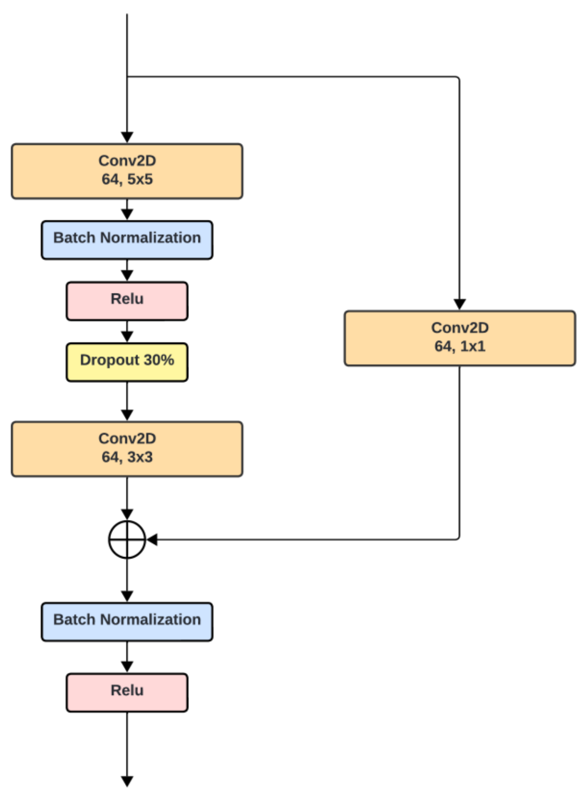

Figure 3. Description of modified ResNet unit. It incorporates Dropout layer for prevents overfitting.

Our model use an adaptation of ResNet units (He et al., 2015) combined with Batch Normalization, and Dropout layers to prevent overfitting. To reduce dimensionality between layers, we employ MaxPooling layers. In the ResNet units, we use ReLU activation along with GlorotUniform kernel initializers.

At the output of the ResNet units, we connect an LSTM layer with 256 units. This layer has no output activation, meaning it uses a linear activation function. At the end of the LSTM layer, we add a Dense layer with 256 units and a linear activation for our regression task.

Table 2. Description of our ML model.

Layer Name	Input Shape	Output Shape
Input	(None, 5, 256, 256, 2)	(None, 5, 256, 256, 2)
Gaussian_noise	(None, 5, 256, 256, 2)	(None, 5, 256, 256, 2)
resnet_dropout_1	(None, 5, 256, 256, 2)	(None, 5, 256, 256, 32)
resnet_dropout_2	(None, 5, 256, 256, 32)	(None, 5, 256, 256, 32)
resnet_dropout_3	(None, 5, 256, 256, 32)	(None, 5, 256, 256, 32)
max_pooling_2d_1	(None, 5, 256, 256, 32)	(None, 5, 64, 64, 32)
resnet_dropout_4	(None, 5, 64, 64, 32)	(None, 5, 64, 64, 64)
resnet_dropout_5	(None, 5, 64, 64, 64)	(None, 5, 64, 64, 64)
max_pooling_2d_2	(None, 5, 64, 64, 64)	(None, 5, 16, 16, 64)
resnet_dropout_6	(None, 5, 16, 16, 64)	(None, 5, 16, 16, 128)
resnet_dropout_7	(None, 5, 16, 16, 128)	(None, 5, 16, 16, 128)
max_pooling_2d_3	(None, 5, 16, 16, 128)	(None, 5, 4, 4, 128)
resnet_dropout_8	(None, 5, 4, 4, 128)	(None, 5, 4, 4, 256)
resnet_dropout_9	(None, 5, 4, 4, 256)	(None, 5, 4, 4, 256)
max_pooling_2d_4	(None, 5, 4, 4, 256)	(None, 5, 1, 1, 256)
Reshape	(None, 5, 1, 1, 256)	(None, 5, 256)
Lstm_1	(None, 5, 256)	(None, 256)
Dense	(None, 256)	(None, 256)
Total parameters		**5 629 728**

Model was trained using a GPU NVIDIA RTX3060 in 75 epochs. The dataset was divided in 80% for training and 20% for test. The training took about 12 hours using a batch size of 4. Adam optimizer (Kingma & Ba, 2014) was used with initial learning rate of 0.005 and decrease rate of factor $\sqrt{2}/_{2}$ each two epochs when validation loss was't improve.. We used log-cosh as our loss function (detailed in section 2.5), where it function loss consider small differences in comparative with MSE (Saleh & Saleh, 2022).. Training and validation loss are showed in Figure 4.

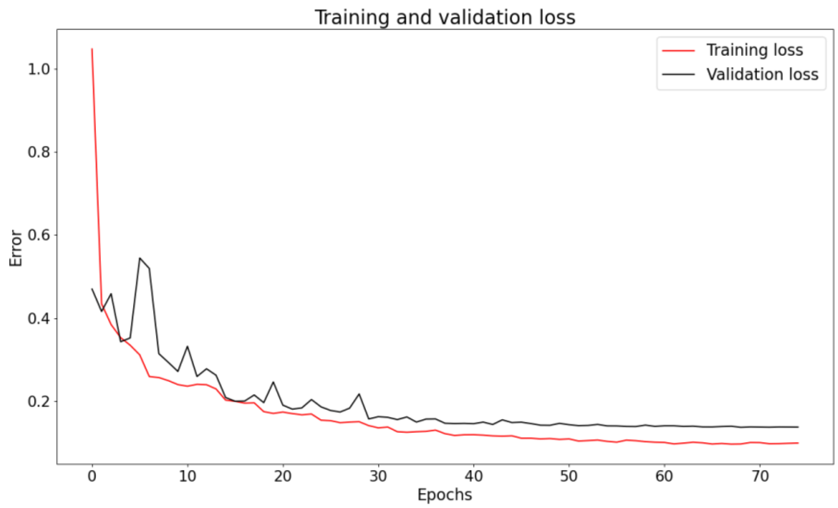

Figure 4. Training and validation loss of our model. The training process lasted 75 epochs, during which the model learned from both datasets.

2.5 Log-Cosh function loss

The loss function is represented in Equation Equation (1) where y_i^p represents the predicted value and y represents the true value. This function loss has a better penalization in small differences in comparative with others function loss as median square error (MSE) or median absolute error (MAE) (Saleh & Saleh, 2022).

$$L(y, y^p) = \sum_{i=1}^{n} \log\left(\cosh\left(y_i^p - y_i\right)\right) \qquad \textit{Equation (1)}$$

2.6 Pearson correlation

To quantify the linear relationship in our series, we use the Pearson correlation. For two series X_1 y X_2 , the correlation is defined in Equation (2) where $\overline{X_1}$ and $\overline{X_2}$ represent the respective mean.

$$r = \frac{\sum(X_1 - \overline{X_1})\,(X_2 - \overline{X_2})}{\sqrt{\sum(X_1 - \overline{X_1})^2}\,\sqrt{\sum(X_2 - \overline{X_2})^2}} \qquad \textit{Equation (2)}$$

The value of r lies in the range [-1,1]. A value of $r = 1$ indicates a perfect positive correlation between the two series. When $0 < r < 1$, it indicates a positive correlation. A value of 0, means there is no linear correlation between the series. When $-1 < r < 0$, it indicates a negative correlation, with r equal to -1 representing a perfect negative correlation.

2.7 Error quantification

To quantify the percentage error with respect to frequency and height values, we used a modified percentage error that incorporates the range R of the corresponding variable. Let $\hat{y}$ be the estimated value and y the true value. The error is computed as:

$$e = \frac{|\hat{y} - y|}{R} * 100\% \qquad \textit{Equation (3)}$$

Where R corresponds to the full range of the variable being evaluated (e.g., 0-25 MHz for frequency, 0-1000 km for height).

3 Results and discussions

3.1 Validation dataset analysis

We evaluated and analyzed the error in the validation dataset for the hmF2 and foF2 parameters. In Figure 5 we show four ionograms contaminated with Spread-F. Polarization X and O were represented with red and purple colors respectively. There are two superimposed curves in each ionogram image, where "LSTM" label represents the frequency profile obtained from our ML model. Besides, "Correct" label represents the ionogram scaled and corrected using SAOExplorer. This representation allows us to evaluate the performance about the fit adjust with the correct curve.

Table 3. Errors in estimation of foF2 and hmF2 parameters

Ionogram	Type ionogram	foF2 error	hmF2 error
Figure 5a	SSF	0.92%	0.78%
Figure 5b	FSF	1.96%	1.5%
Figure 5c	Clear	0.3%	1.18%
Figure 5d	Clear	0.1%	0%

In the figures shown, we observe a strong similarity between the curves obtained by our ML model and the corrected values from the validation dataset. However, there is a small variable offset of up to 1.25 MHz in certain sections of the curves.

In Table 2, we show the estimation errors in percentage with foF2 and hmF2 parameters. Errors were calculated as mentioned in section 2.7. The foF2 parameter error remains below 0.5 MHz, even in the presence of Spread-F type SSF (Figure 5a). The hmF2 parameter had high errors when ionograms were type clear but curves showed high similarity, where maximum absolute error was 11.8 km.

In the next section, we will analyze a new dataset collected weeks after the training process.

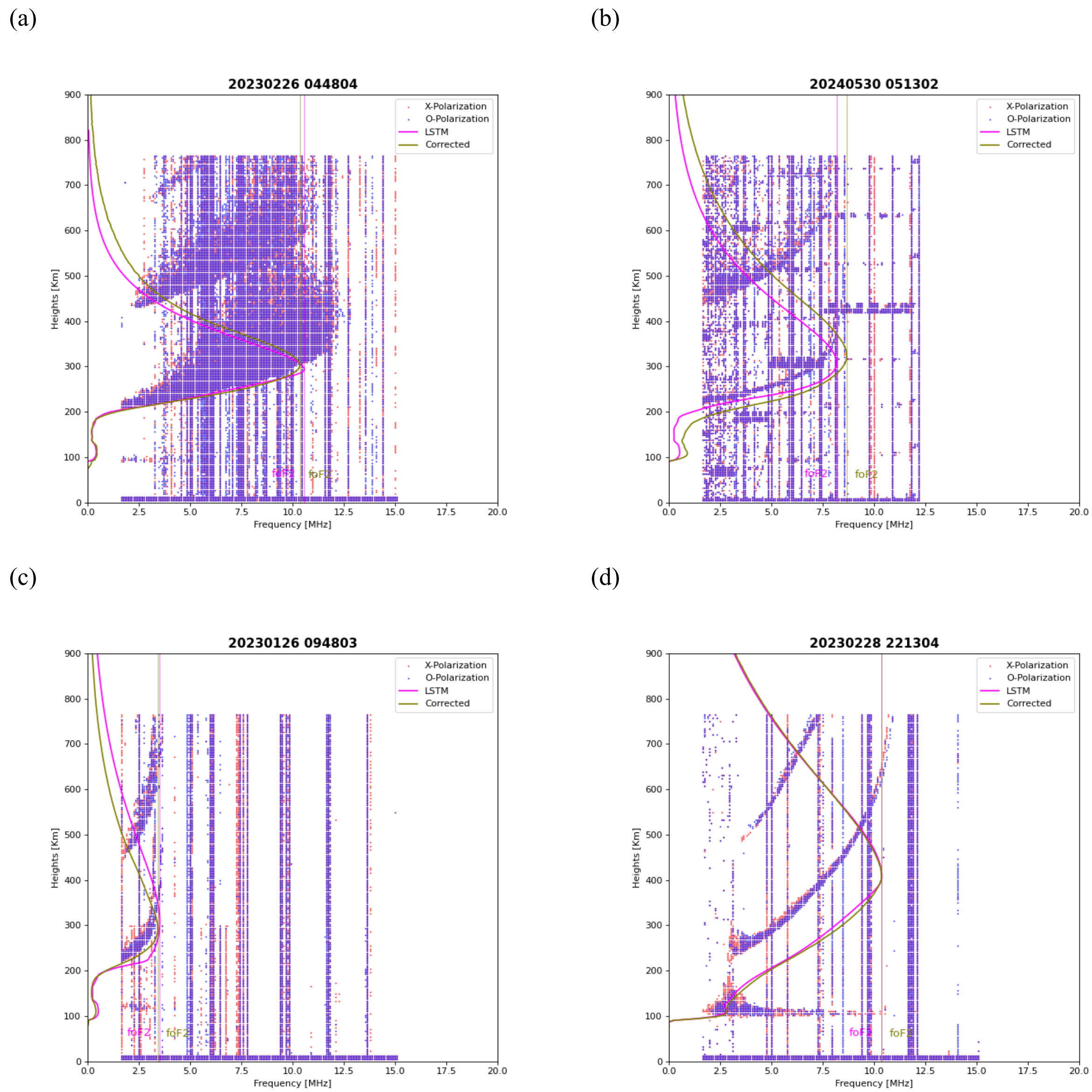

Figure 5. Ionograms obtained from the validation dataset: (a) ionogram containing Spread-F type SSF, and (b) ionogram of FSF type. In (c) and (d) are clear ionograms where (c) contains a short foF2 in comparative with (d).

3.2 Analysis of new data

In this section, we evaluate the performance of our ML model using new data collected during the weeks following the training period. Comparisons were made to assess estimation errors. The collected data corresponds to the Jicamarca ionosonde from the VIPIR network. Two date ranges were selected, containing events related to magnetic storms and Spread-F (described in Table 4).

Table 4. Details of selected events.

Event	Range	Description
Event with magnetic storm	January 1 to January 4, 2025.	Storm magnetic with Kp 8

Event with Spread-F	January 10 to January 11, 2025.	Presence of Spread-F between 20:00 and 00:00 UTC-5

3.2.1 Event with magnetic storm

From January 1st to 4th, 2025, an severe magnetic storm (G4) was observed with Kp equal to 8, where the regional Dst index from Perú indicates that the horizontal magnetic field decayed with a peak of -265.1 nT at 16:00 UTC on January 1st. Regional Dst values were obtained from (Instituto Geofísico del Perú, 2024). The purpose of this comparison is to observe the variations in the foF2 and hmF2 parameters during intense storms, as described in (Cipagauta-Lara & Durand-Manterola, 2010). In addition, we aim to assess whether our ML model is capable of capturing these variations in the frequency profiles.

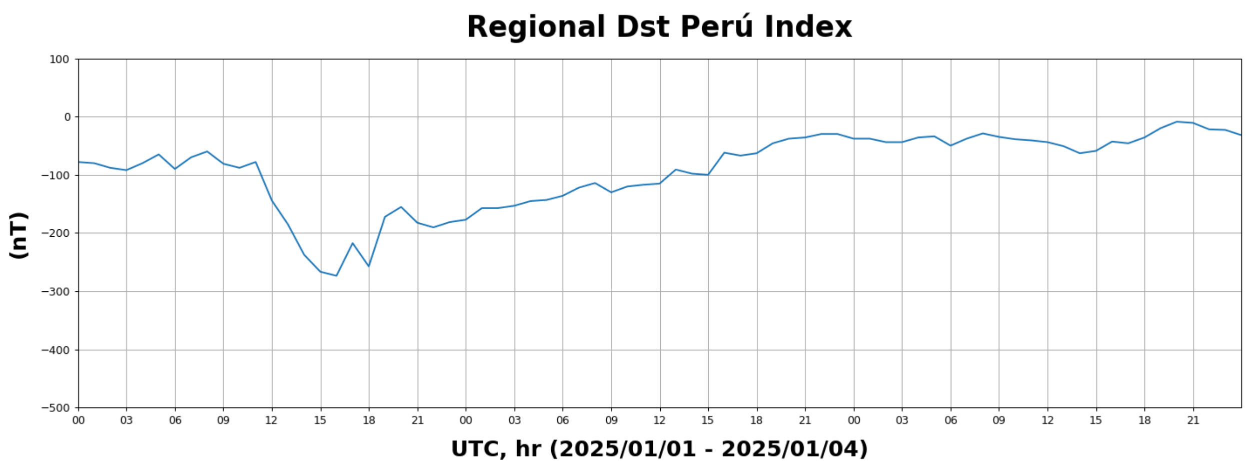

Figure 6. DST Index obtained from WDC for Geogmagnetism, Kyoto for January 2025. Magnetic storms were registered in January 1st with a peak of -221 nT.

We obtain the frequency profiles using our ML model for the analyzed date range, which are shown in Figure 7b. Similarly, we generate the frequency profiles automatically using the ARTIST 5.0 throught SAOExplorer, for the same period (see Figure 7a). In both figures, a black line is drawn to represent the hmF2 parameter. It is important to note that the profiles obtained with the ARTIST 5.0 have not been manually corrected. For this reason, there are gaps or vertical black bands in zones when was challeging for the ARTIST 5.0 estimate a profile.

From the frequency profiles generated by both models, we extract the hmF2 and foF2 parameters, whose values are compared in Figure 8. Analysis of the compared parameters reveals that our ML model exhibits greater stability in its estimates compared to the ARTIST 5.0 model, which shows higher variance during nighttime, when Spread-F occurs. The Pearson correlation coefficient between the hmF2 and foF2 series is 0.68 and 0.71, respectively.

When analyzing the relationship between the DST series and the hmF2 parameter, we observe that the decrease in hmF2 begins around 16:00 UTC, reaching its lowest point due to the magnetic storm at 18:00 UTC. This suggests a visual correlation between the decrease in the Dst index and the behavior of the hmF2 parameter as suggested in (Cipagauta-Lara & Durand-Manterola, 2010). Besides, our model is capable to capture this variations in the ionosphere. However, a detailed statistical analysis of this variation is beyond the scope of this study.

(a)

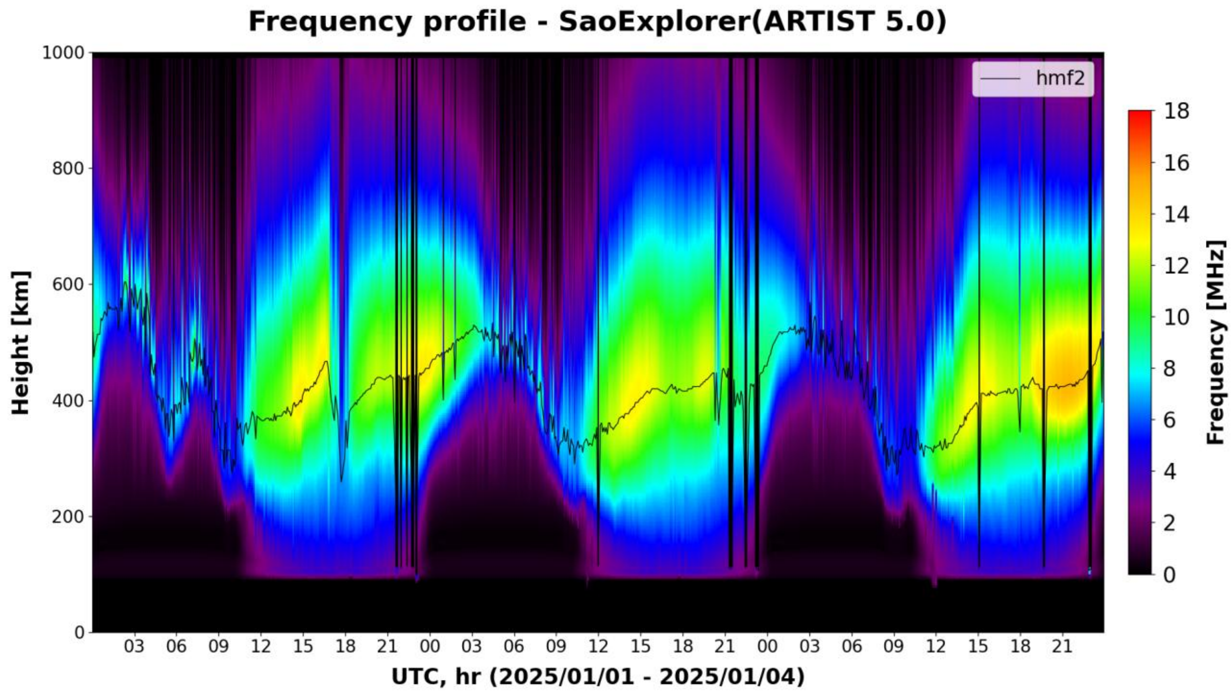

(b)

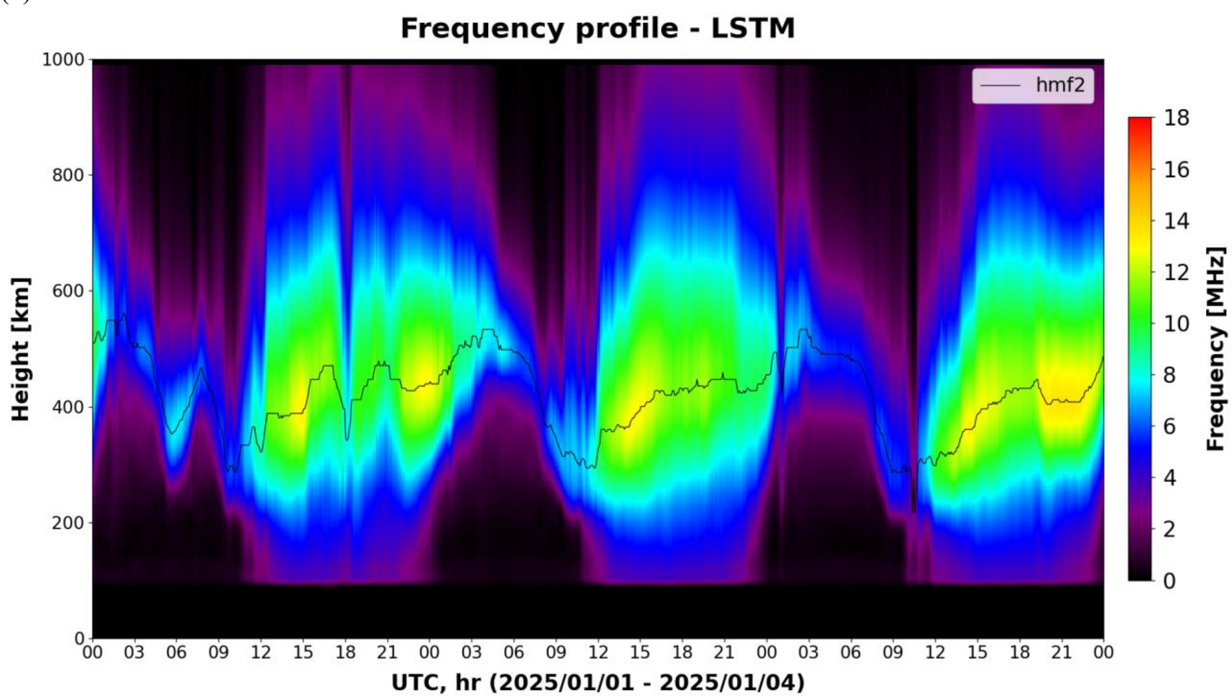

Figure 7. Frequency profiles obtained automatically using ARTIST 5.0 (top) and obtained with our ML model (below) for 1-4 January 2025. Black line represents hmF2 parameter.

(a)

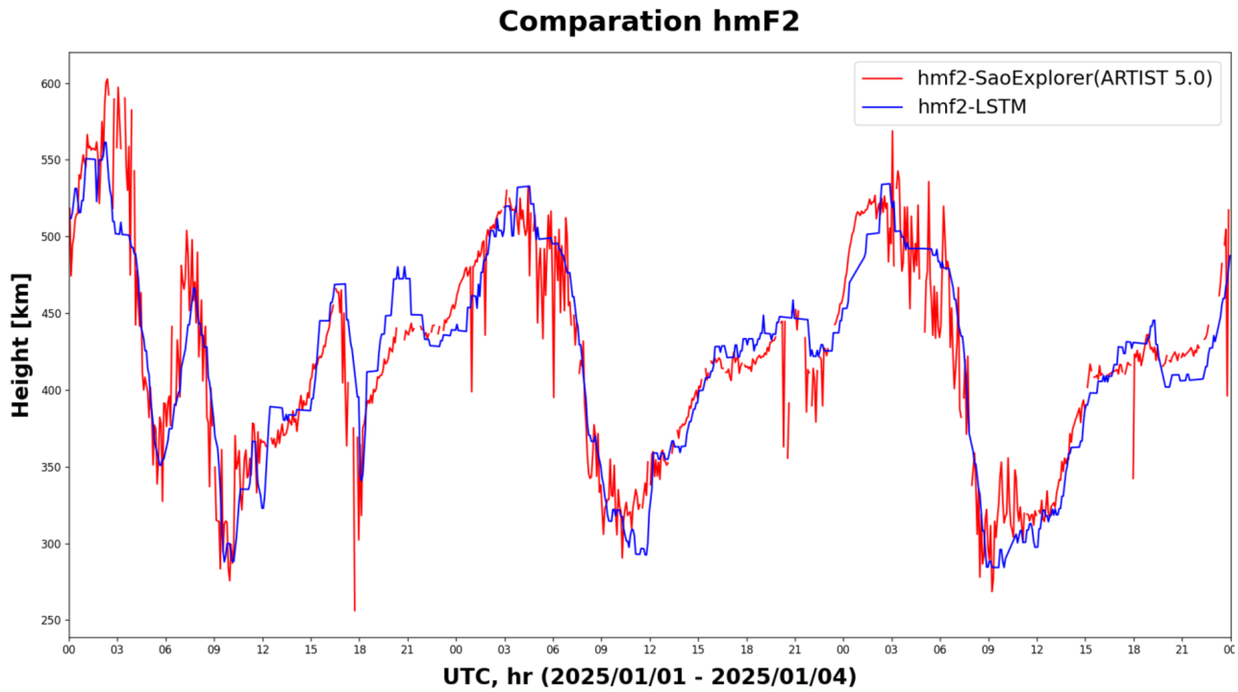

(b)

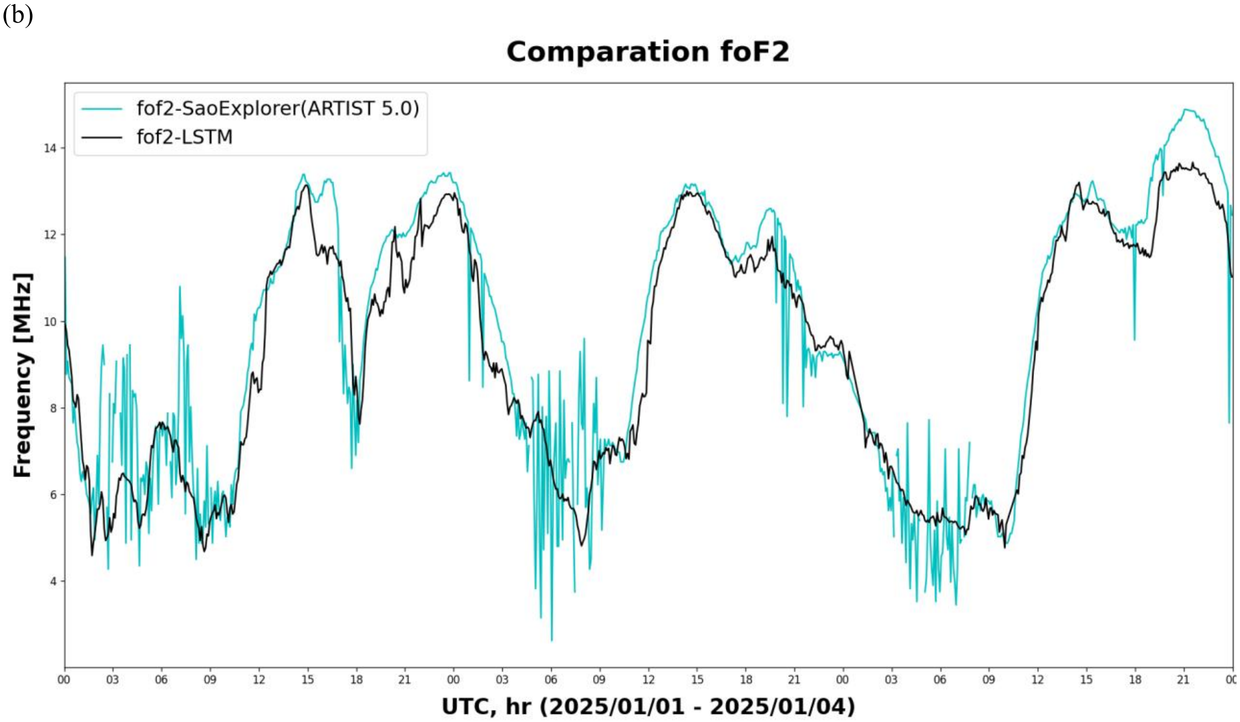

Figure 8. Time series for foF2 and hmF2 parameter obtained from our ML model and ARTIST 5.0 labeled with "LSTM" and "SaoExplorer" respectively. Where series obtained from ARTIST 5.0 shows high variance at night in local time.

3.2.2 Event with Spread-F

Covering the period from January 10 to 11, 2025 (UTC), the Spread-F event extends from approximately 20:00 UTC-5 on January 9 to 03:00 UTC-5 on January 10. A total of 288 ionograms were obtained, including ionograms exhibiting various types of Spread-F (SSF, RSF, FSF). Frequency profiles were obtained automatically with ARTIST 5.0

(without manual correction, see Figure 9a). These profiles were then manually corrected for each ionogram (Figure 9b). In addition, frequency profiles were also obtained using our ML model (Figure 9c).

Figure 9a shows that frequency profiles from the ARTIST 5.0 present outliers and high distortion during the period affected by the Spread-F phenomenon. This distortion is also evident in the foF2 and hmF2 values shown in Figure 10, particularly between 00:00 and 06:00 UTC, where a high degree of variability and outliers is observed when compared to the other two models. The Pearson correlation coefficient between the corrected profiles and those from our model is 0.98, while the correlation with the profiles from ARTIST 5.0 is 0.71.

(a)

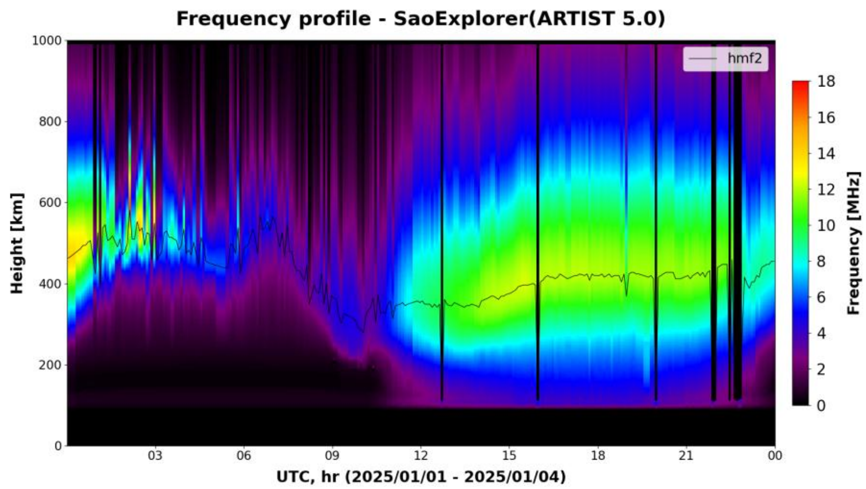

(b)

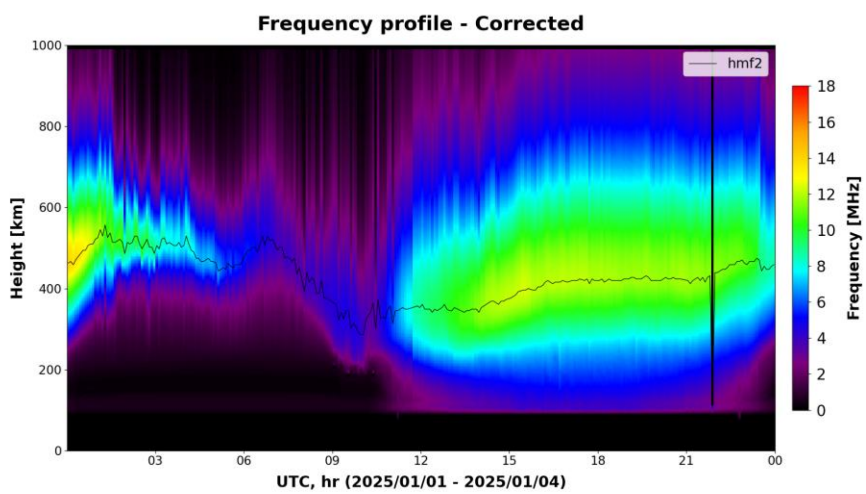

(c)

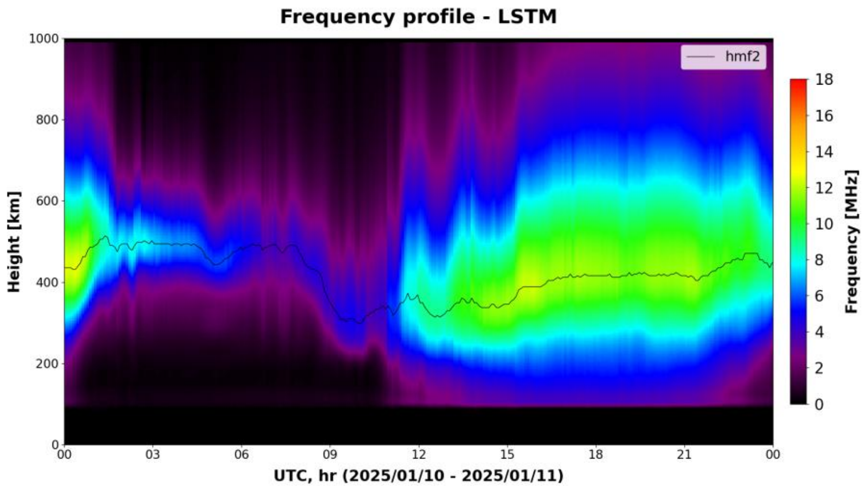

Figure 9. Frequency profiles obtained for the same time. In (a) profiles were obtained automatically without correction using ARTIST 5.0. There are many black stripes due to difficulties in estimation for the ARTIST 5.0. In (b) profiles were corrected manually. In (c) profiles were obtained with our model ML. Black line represents hmF2 parameter.

(a)

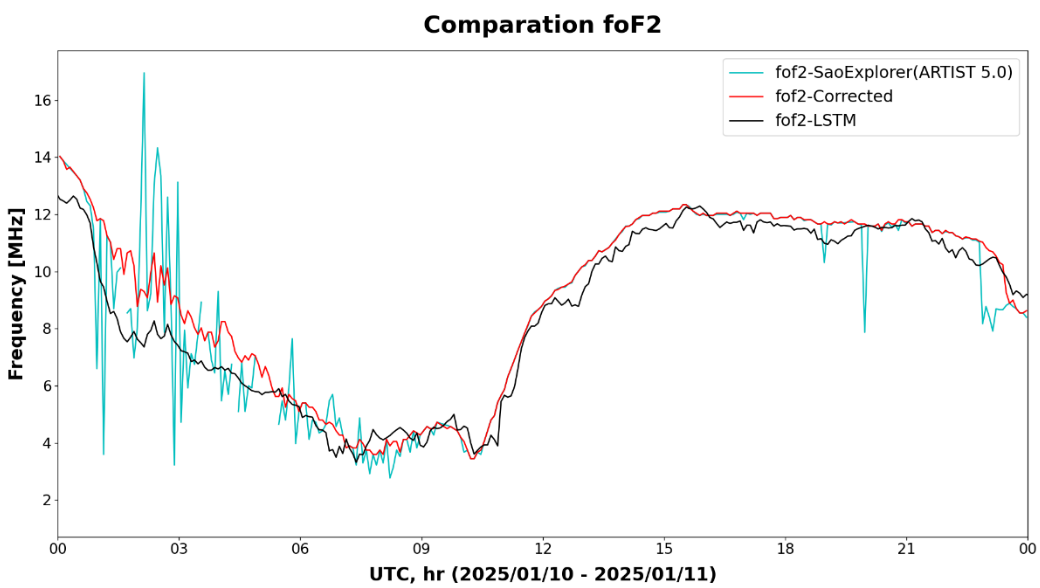

(b)

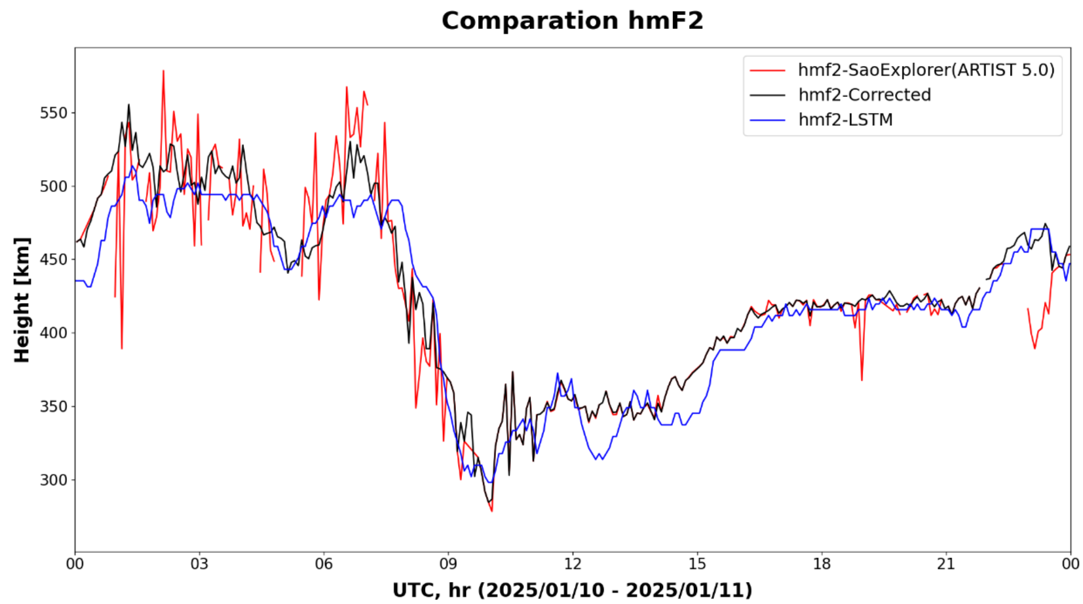

Figure 10. Time series for foF2 and hmF2 parameter obtained from our ML model, ARTIST 5.0 and profiles corrected manually, labels correspond to "LSTM", "SaoExplorer" and "Corrected" respectively. Where serie obtained from ARTIST 5.0 shows high variance at night in local time. The corrected data and our model's results are closely similar.

We analyze the ionogram recorded at 02:08:04 UTC (see Figure 11a), which corresponds to an ionogram affected by Spread-F of the SSF type. The figure displays the ionogram with a frequency scale ranging from 0 to 20 MHz and a height scale from 0 to 1000 km. Echoes of the O- and X-polarizations are represented by red and purple dots, respectively. The frequency profiles obtained from our ML model, the ARTIST 5.0 model, and the manually corrected profiles are labeled as 'LSTM', 'SaoExplorer', and 'Corrected', respectively.

It can be observed that the frequency profile automatically generated by the ARTIST 5.0 model differs by more than 5 MHz in the foF2 parameter compared to the other profiles. The absolute error in the foF2 and hmF2 parameters between the profile produced by our model and the manually corrected profile is 1.94 MHz and 15.44 km, respectively.

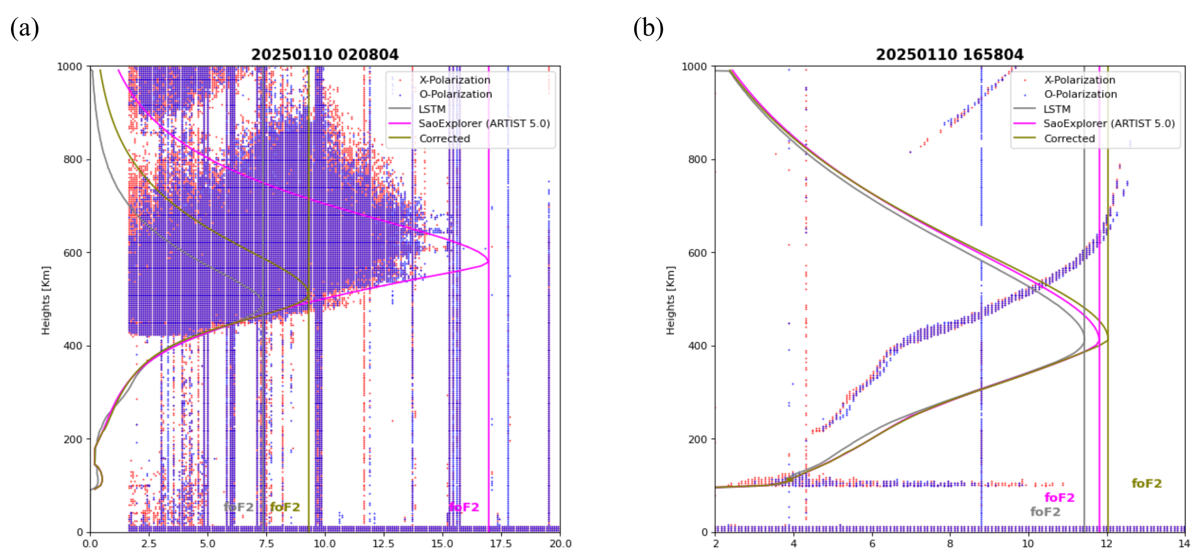

Figure 11. Comparation of different profiles obtained from a same ionogram where labels represents for ARTIST 5.0, manually corrected and our model ML for "SaoExplorer", "Corrected" and "LSTM" respectively. In (a) corresponds to an SSF ionogram, and (b) to a clear ionogram. In both cases, our model closely matches the corrected profile.

As a comparison at a different time, we randomly selected the ionogram recorded at 16:58:04 UTC (see Figure 11b), which shows no presence of Spread-F. In this case, the three compared frequency profiles appear relatively similar; the best-scaled profile is the one that most closely follows the end of the echo. For this ionogram, that corresponds to the ARTIST 5.0 profile.

The ARTIST 5.0 shows a closer match to the manually corrected profile, with absolute errors of 0.22 MHz in foF2 and 3.32 km in hmF2. In comparison, the frequency profile generated by our ML model presents slightly higher errors of 0.6 MHz and 1.56 km for foF2 and hmF2, respectively. This example illustrates that the ARTIST 5.0 model performs slightly better in accurately fitting the frequency profile under non-disturbed conditions.

5 Conclusions

In this paper, we present a novel methodology for obtaining frequency profiles using a Machine Learning model, allowing for the extraction of key parameters such as foF2 and hmF2, as well as frequency profiles in the range of 80 to 1000 kilometers, based on ionograms recorded by the VIPIR ionosonde.

In comparison with the ARTIST 5.0, our proposed model demonstrates greater robustness in estimating frequency profiles, even in the presence of various types of Spread-F. In contrast, the ARTIST 5.0 model shows higher errors in the estimation of frequency profiles and related parameters.

This methodology also improves the presentation of ionosonde data from the VIPIR system at the Jicamarca Radio Observatory, where ionograms are processed in real time and the resulting frequency profiles are displayed on the Space Weather website developed by the IGP (Instituto Geofísico del Perú, 2024). Moreover, this approach is applicable to any ionosonde deployed worldwide.

Acknowledgments

This work is carried out at the Jicamarca Radio Observatory, Lima Peru. The Jicamarca Radio Observatory is a facility of the Instituto Geofísico del Perú operated through an agreement with Cornell University, under Prime Agreement AGS-2213849 from the National Science Foundation.

We express our thanks to the Low latitude Ionospheric Sensor Network (LISN) for the VIPIR data. The LISN project is funded by NSF and is led by Boston College in collaboration with the Instituto Geofísico del Perú and other institutions.

References

Abdullah, M., Ahmad, M., & Han, D. (2020). Facial expression recognition in videos: An CNN-LSTM based model for video classification. In *2020 International conference on electronics, information, and communication (ICEIC)* (pp. 1–3). IEEE.

Alshingiti, Z., Alaqel, R., Al-Muhtadi, J., Haq, Q. E. U., Saleem, K., & Faheem, M. H. (2023). A deep learning-based phishing detection system using CNN, LSTM, and LSTM-CNN. *Electronics*, *12*(1), 232.

Benchawattananon, P., Siritaratiwat, A., Supnithi, P., Nishioka, M., Perwitasari, S., Suthisopapan, P., & Kruesubthaworn, A. (2024). Automatic classification of spread-F types in ionogram images using support vector machine and convolutional neural network. *Earth, Planets and Space*, *76*(1), 56.

Cipagauta-Lara, E. C., & Durand-Manterola, H. J. (2010). Efectos de tormentas geomagnéticas sobre la ionosfera de las estaciones El Cerrillo (Toluca, México) y Boulder (Colorado, EUA). *Revista Mexicana de Ciencias Geológicas*, *27*(2), 366–373. Retrieved from http://www.scielo.org.mx/scielo.php?script=sci_arttext&pid=S1026-87742010000200016&lng=es&nrm=iso

De la Jara, C., & Olivares, C. (2021). Ionospheric echo detection in digital ionograms using convolutional neural networks. *Radio Science*, *56*(8), 1–15.

Galkin, I. A., Khmyrov, G. M., Kozlov, A. V., Reinisch, B. W., Huang, X., & Paznukhov, V. V. (2008). The artist 5. In *AIP conference proceedings* (Vol. 974, pp. 150–159). American Institute of Physics.

Gong, Y., Zhang, Y., Wang, F., & Lee, C.-H. (2024). Deep learning for weather forecasting: A cnn-lstm hybrid model for predicting historical temperature data. *arXiv Preprint arXiv:2410.14963*.

Gopi Krishna, S., Valladares, C., Doherty, P., Bullet, T., & Livingston, R. (2009). Studies of equatorial spread-F using LISN VIPIR.

Graves, A., & Graves, A. (2012). Long short-term memory. *Supervised Sequence Labelling with Recurrent Neural Networks*, 37–45.

He, K., Zhang, X., Ren, S., & Sun, J. (2015). Deep Residual Learning for Image Recognition. Retrieved from https://arxiv.org/abs/1512.03385

Instituto Geofísico del Perú. (2024). Radio Observatorio de Jicamarca: Datos DST. Retrieved from https://www.igp.gob.pe/observatorios/radio-observatorio-jicamarca/?page_id=11880

Kim, S., Hong, S., Joh, M., & Song, S. (2017). Deeprain: Convlstm network for precipitation prediction using multichannel radar data. *arXiv Preprint arXiv:1711.02316*.

Kingma, D. P., & Ba, J. (2014). Adam: A method for stochastic optimization. *arXiv Preprint arXiv:1412.6980*.

Masahito, N., Masahisa, S., Toyohisa, K., Toshihiko, I., & Yukinobu, K. (2015). Geomagnetic Dst index. *Geomagnetic Dst Index*.

Moradi, R., Berangi, R., & Minaei, B. (2020). A survey of regularization strategies for deep models. *Artificial Intelligence Review*, *53*(6), 3947–3986.

Pan, B., Yu, H., Cheng, H., Du, S., Cai, S., Zhao, M., et al. (2023). A CNN–LSTM machine-learning method for estimating particulate organic carbon from remote sensing in lakes. *Sustainability*, *15*(17), 13043.

Penndorf, R. (1962). Classification of spread-F ionograms. *Journal of Atmospheric and Terrestrial Physics*, *24*(9), 771–778.

Saleh, R. A., & Saleh, A. (2022). Statistical properties of the log-cosh loss function used in machine learning. *arXiv Preprint arXiv:2208.04564*.

Santos, C. F. G. D., & Papa, J. P. (2022). Avoiding overfitting: A survey on regularization methods for convolutional neural networks. *ACM Computing Surveys (Csur)*, *54*(10s), 1–25.

Sherstyukov, R., Moges, S., Kozlovsky, A., & Ulich, T. (2024). A deep learning approach for automatic ionogram parameters recognition with convolutional neural networks. *Earth and Space Science*, *11*(10), e2023EA003446.

Srivastava, N., Hinton, G., Krizhevsky, A., Sutskever, I., & Salakhutdinov, R. (2014). Dropout: a simple way to prevent neural networks from overfitting. *The Journal of Machine Learning Research*, *15*(1), 1929–1958.

Valladares, C., & Chau, J. (2012). The low-latitude ionosphere sensor network: Initial results. *Radio Science*, *47*(04), 1–18.

Wang, G., Shi, J., Wang, X., & Shang, S. (2008). Seasonal variation of spread-F observed in Hainan. *Advances in Space Research*, *41*(4), 639–644.

Wang, X., Gao, L., Song, J., & Shen, H. (2016). Beyond frame-level CNN: saliency-aware 3-D CNN with LSTM for video action recognition. *IEEE Signal Processing Letters*, *24*(4), 510–514.

Xiao, Z., Wang, J., Li, J., Zhao, B., Hu, L., & Liu, L. (2020). Deep-learning for ionogram automatic scaling. *Advances in Space Research*, *66*(4), 942–950.

Yacoub, M., Pacheco, E. E., Abdelwahab, M., De La Jara, C., & Mahrous, A. (2025). Automatic detection and classification of Spread-F in ionograms using convolutional neural network. *Journal of Atmospheric and Solar-Terrestrial Physics*, *270*, 106504.